# Health monitoring of bearing and gear faults by using a new health indicator extracted from current signals

Moncef Soualhi, Thi Phuong Khanh Nguyen, Abdenour Soualhi, Kamal Medjaher, Kamel Eddine Hemsas

# Health monitoring of bearing and gear faults by using a new health indicator extracted from current signals

Moncef Soualhi [a,*], Khanh T.P. Nguyen [a], Abdenour Soualhi [b], Kamal Medjaher [a], Kamel Eddine Hemsas [c]

[a] Laboratoire Génie de Production, Université de Toulouse, INPT-ENIT, 47 Av. d'Azereix, 65000 Tarbes, France
[b] LASPI, CUR, University of Saint-Etienne, France
[c] LAS, UFAS1, Sétif, Algeria

ARTICLE INFO

*Keywords:*
Bearing and gear faults
Health monitoring
Signal processing
Feature extraction
Health indicator
Machine learning
Artificial intelligence
Fault detection and diagnostics
Motor current signal analysis

ABSTRACT

Gear reducer motors play an important role in industry due to their robustness and simplicity of con struction. However, the appearance of faults in these systems can affect the quality of the product and lead to significant financial losses. Therefore, it is necessary to perform Prognostics and Health Management (PHM) for these systems. This paper aims to develop a practical and effective method allow ing an early fault detection and diagnostic for critical components of the gear reducer, in particular gear and bearing defects. This method is based on a new indicator extracted from electrical signals. It allows characterizing different states of the gear reducer, such as healthy state, bearing faults, gear faults, and combined faults. The diagnostic of these states is done by the Adaptive Neuro Fuzzy Inference System (ANFIS). The efficiency and the robustness of the proposed method are highlighted through numerous experimental tests with different levels of loads and speeds.

## 1. Introduction

Gear reducer motors are widely used in industrial applications due to their robustness and low cost. However, during their life cycle, different degradation types can occur in these systems lead ing to undesirable situations such as: system degradation, down time, high maintenance costs, product quality damages, etc. Therefore, maintaining such systems in a good condition requires the implementation of an adequate maintenance strategy. The pre dictive maintenance, using Prognostics and Health Management (PHM), can be a good candidate. It ensures, on one side, the relia bility, availability, maintainability and safety of industrial systems [1,2]. And on the other side, it allows the detection and diagnostics of machine faults [1,3]. According to experts statistics, bearing and gear faults represent a significant part of the defects of gear redu cer motors [1,3 5]. Hence, it is essential to adopt efficient monitor ing methods to diagnose their faults.

In literature, fault detection and diagnostics (FDD) approaches can be generally classified into two groups [1,2,6]: model based and data driven based approaches. The model based approaches use mathematical equations to represent the system behavior. It is more accurate than the data driven approaches. However, con sidering the complexity of systems, it is often difficult to imple ment the model based methods. The second group is based on the analysis of signals extracted from different types of sensors. It is suitable for complex systems where no *a priori* knowledge is needed to monitor the system. However, its performance strictly depends on the availability of sufficient and representative data [7]. The choice of an appropriate approach depends on the system knowledge we have on it, and the availability of historical degrada tion data. In reality, it is difficult to model the degradation pro cesses of bearings and gears because of the complexity of their mechanism, which is nonlinear, non stationary and stochastic. Therefore, the data driven approach is chosen because of abundant data acquired by different sensor types [1]. Among them, vibration and current signals are promising and non invasive parameters for monitoring.

The FDD of bearings and gears can be obtained by using the time domain analysis. In this case, statistical features, such as Root Mean Square (RMS), Standard Deviation (StD), Kurtosis (KUR), Skewness (SKE), etc., are extracted from vibration signals to per form condition monitoring [8 10]. On the other hand, the authors in [11 13] propose the use of the frequency analysis to identify the

* Corresponding author.
*E-mail address:* moncef.soualhi@enit.fr (M. Soualhi).

characteristic frequencies of the localized roll bearing defects. Gear fault diagnostic is addressed in [5,13 15]. The authors in [5,13,14] extract fault characteristic frequencies to localize gear defects while the work in [15] uses frequency domain features to detect gear abnormalities. In the time frequency domain, the studies [16 21] propose to use the wavelet transformation methods for the detection of bearing localized faults. In addition, the work in [22] proposes to combine the fast dynamic time warping method and the kurtosis technique for fault detection of gears. The study [23] uses angular measurements to diagnose different gear faults.

In addition to vibration signals, acoustic emission data can be used as an alternative for condition monitoring, as in [24 26]. In these works, the authors show the effectiveness of acoustic signals in motor fault detection and diagnostics, including bearing, gear and electrical faults such as shorted coils. However, fault detection and diagnostic based on acoustic emission signals may be unfeasi ble when the motor runs too quietly [24].

The main drawback of the above studies is that the sensitivity of the vibrations and the acoustic emissions can be reduced due to the industrial environment noises. Therefore, it is difficult to diag nose electrical faults in motors via these signals. Hence, electrical signals (current, voltage, etc.) can be used as a non invasive alter native for bearings and gears health monitoring.

Considering the previous studies, the bearing and gear faults are often separately addressed in the literature. Moreover, to our knowledge, no existing research takes into account numerous operating conditions of motors when considering its different fail ure types, such as bearing faults, gear faults and both component faults in the same time. Therefore, this paper aims to fill this liter ature gap. In detail, a new indicator extracted from the three phase current signals is presented to characterize different system states, as healthy state, bearing faults, gear faults and combined faults of an asynchronous motor driving a geared box, with different levels of loads and speeds. The diagnostic of these classes is done by arti ficial intelligence using the Adaptive Neuro Fuzzy Inference Sys tem (ANFIS). The remainder of the paper is structured as follows. Section 2 presents the proposed methodology to extract and build health indicators. The performance and robustness of our health indicators are highlighted in Section 3 through experimental results carried out on a test bench provided by the LASPI labora tory. Finally, the conclusion and perspective of this work will be presented in Section 4.

## 2. Proposed methodology for fault detection and diagnostics

This section presents the main steps of the proposed methodol ogy for bearing and gear fault detection and diagnostics (Fig. 1).

The system analysis allows identifying the critical components and the corresponding failure mechanisms leading to sensor place ment and data acquisition. The recorded data are then processed to extract relevant features. For this purpose, both of the frequency and the time domain are investigated. In detail, the frequency anal ysis is used for each current signal to extract a characteristic value (the MAX value of the FFT) corresponding to different load varia tion states. On the other hand, the time domain analysis is applied to extract values (such as the peak to peak value of the signal amplitude) that allow tracking the evolution of the bearing and the gear degradations. After that, a new feature is evaluated and used to build health indicators. These indicators are exploited in the third step to identify and classify the different health states of the motor's critical components (healthy state, bearing faults, gear faults, and combined faults). The classification is performed by using pattern recognition methods, which are part of Machine Learning (ML). The following subsections describe in details the above mentioned steps.

### 2.1. From system to data acquisition

One of the main tasks of health monitoring is to identify the appropriate physical parameters to be observed in order to track the system degradation process. To achieve this task, a methodol ogy is proposed and shown in Fig. 2.

At the beginning of the methodology, it is necessary to analyze the architecture, the structure and the functionalities of the system in order to determine the critical components leading to system failure. For this purpose, numerous approaches can be used such as experience feedback, fault tree, event tree, cause and effect tree, etc. [1]. In the framework of this paper, we focus on asynchronous motors. According to the studies in [1,3,27], bearing failures repre sent 41 45% of faults in the induction motors. Moreover, according to the studies presented in [4,5], gear defects are also the main cause that leads to wind turbines or gear reducer motor failures. Therefore, bearings and gears can be considered as the motor crit ical components whose health states should to be monitored over time to detect and diagnose their faults. To do this, it is important to determine the most suitable physical parameters for health monitoring. According to the studies presented in [3 5,8,9], the vibration signal is the most used data to track the bearing and gear degradations. However, the sensitivity of this type of signal can be reduced due to noises in operational environments. Furthermore, one of the major disadvantage of vibration monitoring is its high cost of the accelerometers and the difficulties when accessing to the machine to install the sensors. Besides, the electrical sensors are inexpensive and easy to implement. Therefore, current sensors, which are considered as a non invasive way of monitoring the motors, are used in this paper. This is also known as Motor Current Signal Analysis (MCSA) [28].

### 2.2. From data to features extraction and health indicators construction

This subsection deals with the extraction of a new health indi cator from the three phase current signals. The extracted health indicator will be used to detect and diagnose bearing and gear defects in gear reducer motors. The extraction process is shown in Fig. 3.

Compared to what is reported in the literature [1,8,15,16,24,26], the health indicator proposed in this paper is robust when taking into account the impact of different load levels variation on the machine. Also, this indicator allows detecting both bearing and gear faults simultaneously. The main steps of the features extrac tion and health indicators construction are presented hereafter.

1. **Data acquisition.** Depending on the operating conditions of the motor, the three phase raw current signals ($i_a(t)$, $i_b(t)$, and $i_c(t)$) are used to extract the relevant features. These raw signals are shown in Fig. 4.
2. **Splitting every current signal into $N$ segments of length $L$.** The obtained signals are split into several segments of length $L$. In this contribution, each recorded signal equals to 10 s and is split into 100 segments of 0.1 second ($L$ 0.1 s, $N$ 100). Each signal segment is denoted by $y_{jh}$ (Fig. 5) where $j$ character izes the phase current ($j \in [a, b, c]$) and $h$ represents the segment number ($h \in [1, \ldots, N]$). This step aims to reduce the data size for signal processing, and takes only the relevant features, such as the peak to peak and the amplitude maximum values from the observations.
3. **Extraction of features from every segment observations $y_{jh}$.** This step is inspired from the result in [29]. In practice, there exits a large dispersion in the observations of the health indica tors which characterize the system's health states. Therefore, it

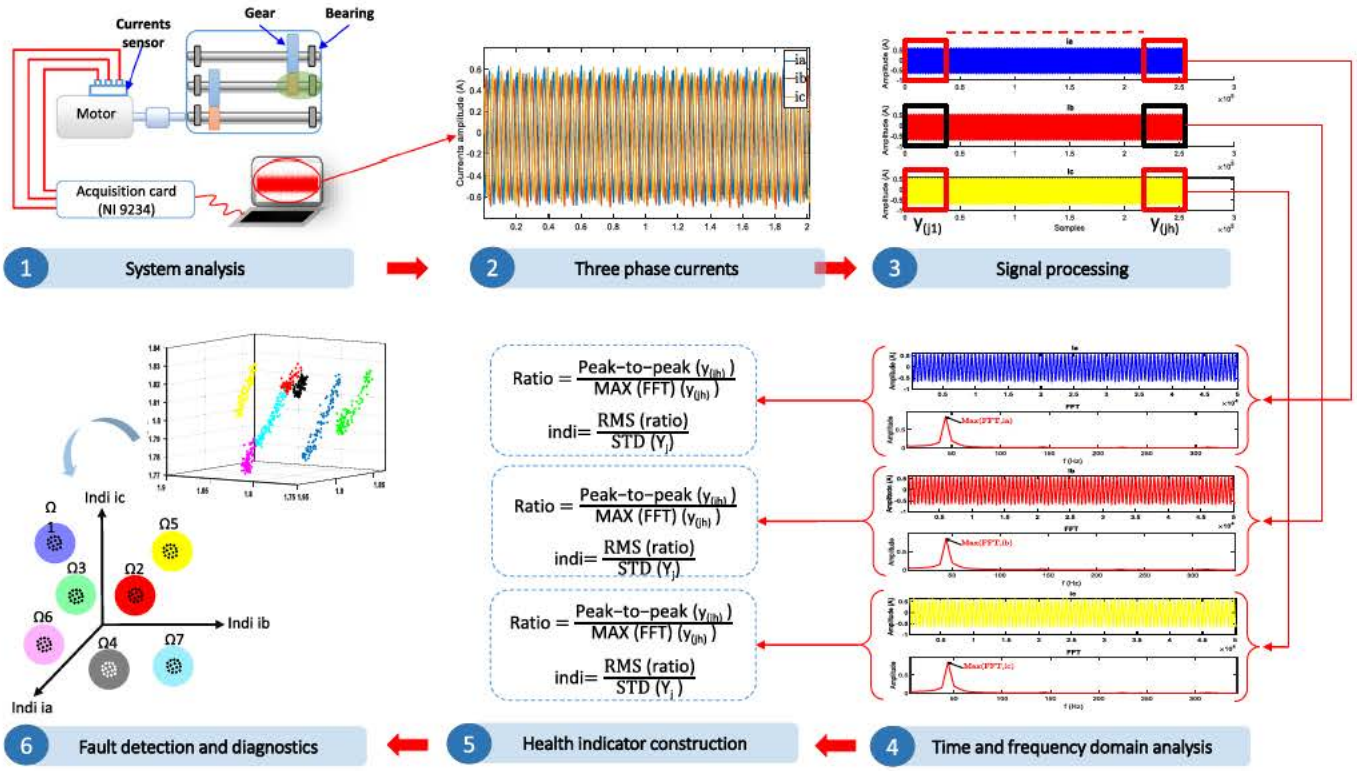


**Fig. 1.** The proposed methodology for FDD of gear reducer motors.

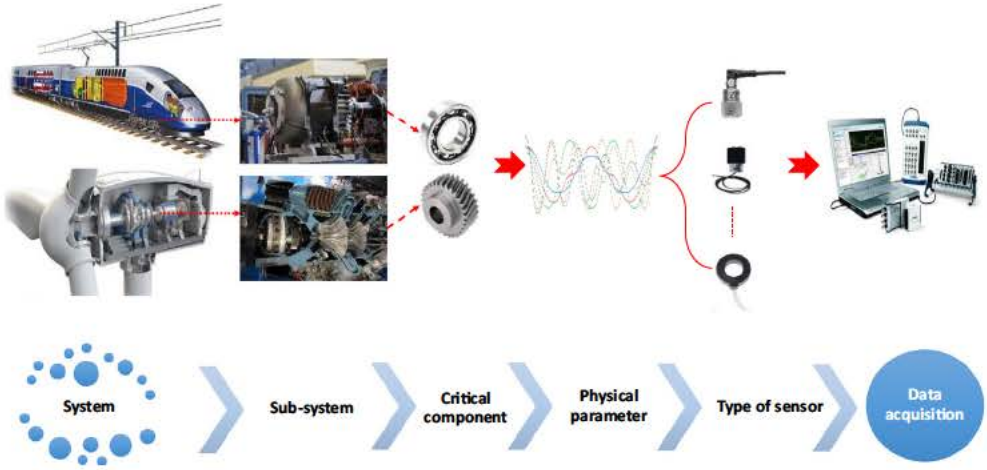


**Fig. 2.** From system to data acquisition.

is necessary to calculate the ratio between the peak to peak values of each segmented signal in time domain ($y_{jh}$) and its spectral amplitude in frequency domain (MAX(FFT($y_{jh}$)). This ratio allows grouping all the observations of the different load levels (e.g. 0%, 25%, 50%, 75%) in one class. Figs. 6 and 7 illustrate the dispersion problem and the effectiveness of the ratio, respectively.

In detail, Fig. 6 shows an example of the distribution of the health indicators observations. These health indicators repre sent three different health states (e.g. healthy, faulty 1, faulty 2) without the normalization to the MAX(FFT($y_{jh}$)) value. Each health state contains several groups of observations, which cor respond to different load levels (e.g. 0%, 25%, 50%, 75%). Fig. 7 shows the effect of the normalization on the reduction of the observations dispersion caused by the load level variations.

The Fig. 8 shows the frequency and the time domain plots of the recorded signal. These plots allow separating the classes by a decision making rule. This rule is based on the values of the ratio between $y_{jh}$ amplitudes and MAX($y_{jh}$(f)), which are then used to represent each health state (regrouping different load level observations, in Fig. 6) by a class as illustrated in Fig. 7.

$$z_{jh} \quad \frac{y_{jh}}{\mathrm{MAX}(y_{jh}(f))}; \quad \text{where } y_{jh}(f) \quad \mathrm{FFT}(y_{jh}) \tag{1}$$

The proposed indicator is then expressed by the ratio between the RMS value of each segment $z_{jh}$ and the standard deviation StD of the total raw signal $Y_j$.

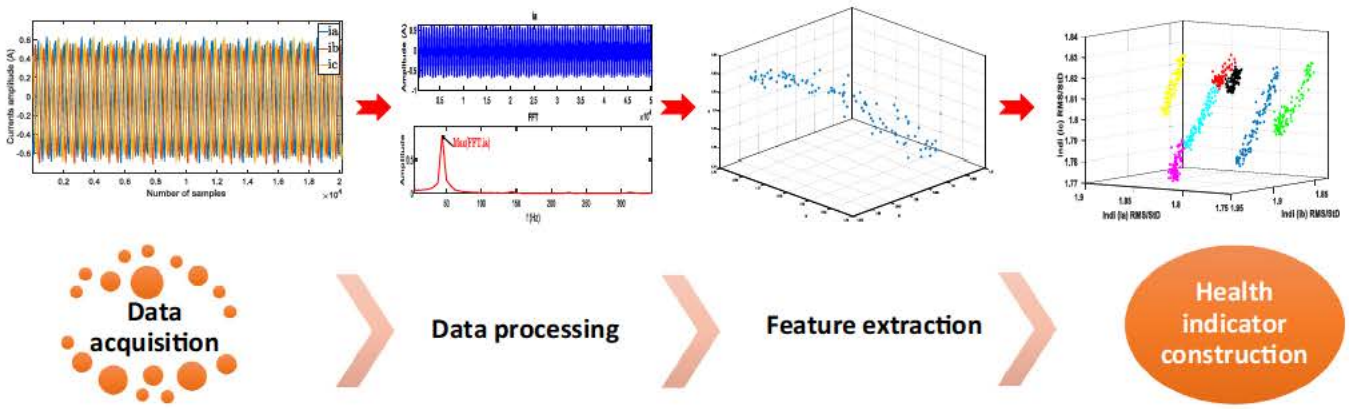


**Fig. 3.** From data to features extraction and health indicators construction.

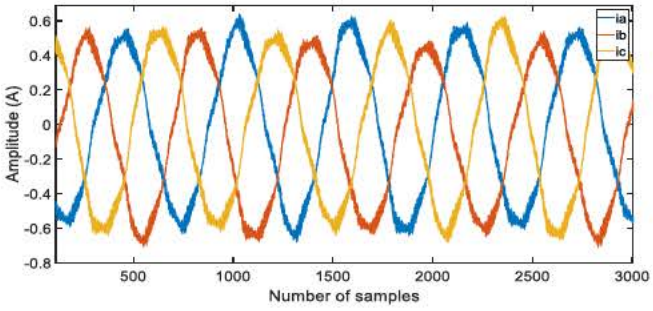


**Fig. 4.** Three-phase raw current signals.

$$indi_{jh} \quad \frac{\mathrm{RMS}(z_{jh})}{\mathrm{StD}(Y_j)} \tag{2}$$

where $z_{jh}$ is the $h^{th}$ signal segment of the $j^{th}$ phase, $z_{jh}$ and $Y_j$ con sist of *ne* and *Ne* sampling points, respectively. The RMS and the StD are respectively the root mean square and the standard devi ation. The RMS value measures the average energy of the signal, each degradation will vary the RMS values [30]. On the other hand, the StD value allows to limit the dispersion between the indicators of different health states.

$$\mathrm{RMS}(z_{jh}) \quad \sqrt{\frac{1}{ne} \times \sum_{n\ 1}^{ne} z_{jh}(n)^2} \tag{3}$$

$$\mathrm{StD}(Y_j) \quad \sqrt{\frac{1}{Ne} \times \sum_{n\ 1}^{Ne} \left( Y_j(n) \quad Y_j \right)^2} \tag{4}$$

4. **Construction of health indicators.** The obtained indicator is then exploited to build health indicators which are used to classify, detect and diagnose the bearing and gear faults. Note that the utilization of only one indicator is not suffi cient to detect several faults. In this case, the combination of different indicators is necessary to move from one dimensional space to three dimensional space by using a pattern recognition technique as shown in Fig. 9.
This technique is based on classifying N observations denoted $(indi_{iah}, indi_{ibh}, indi_{ich})$ into classes where $h \in [1, \ldots, N]$. Each observation is characterized by a vector including the three health indicators corresponding to the three phase current signals of the motor. This vector is then used to build a matrix of health indicators as illustrated hereafter.

$$indi \quad \begin{bmatrix} indi_{ia1} & indi_{ib1} & indi_{ic1} \\ indi_{ia2} & indi_{ib2} & indi_{ic2} \\ indi_{ia3} & indi_{ib3} & indi_{ic3} \\ \cdots & \cdots & \cdots \\ \cdots & \cdots & \cdots \\ indi_{iaN} & indi_{ibN} & indi_{icN} \end{bmatrix}$$

### 2.3. From health indicators to fault detection and diagnostics

This step aims to map each value of the above matrix to a cor responding class (e.g. healthy, degraded, faulty, etc.) by using a pattern recognition technique. This technique is based on a classi fier model using a training database for the recognition of the membership class of each observation. Note that this technique requires *a priori* knowledge of the classes for the construction of

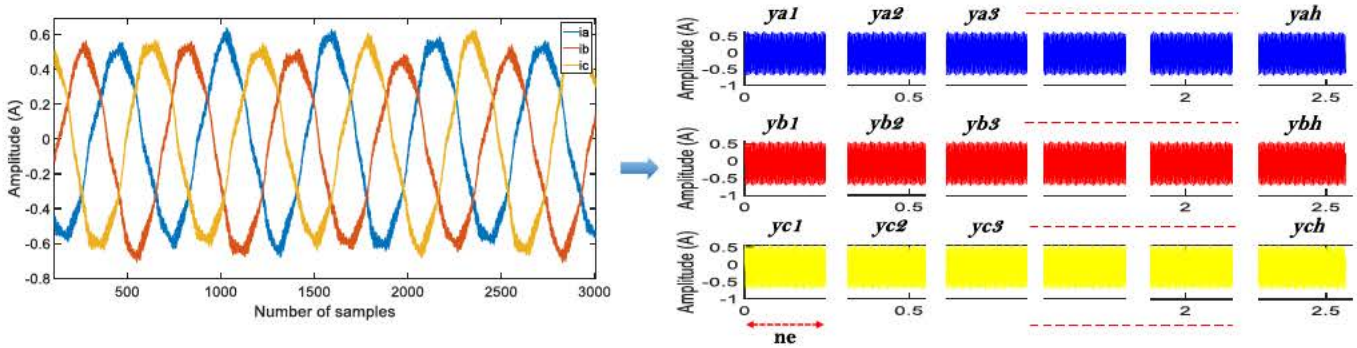


**Fig. 5.** Sampling the current signals.

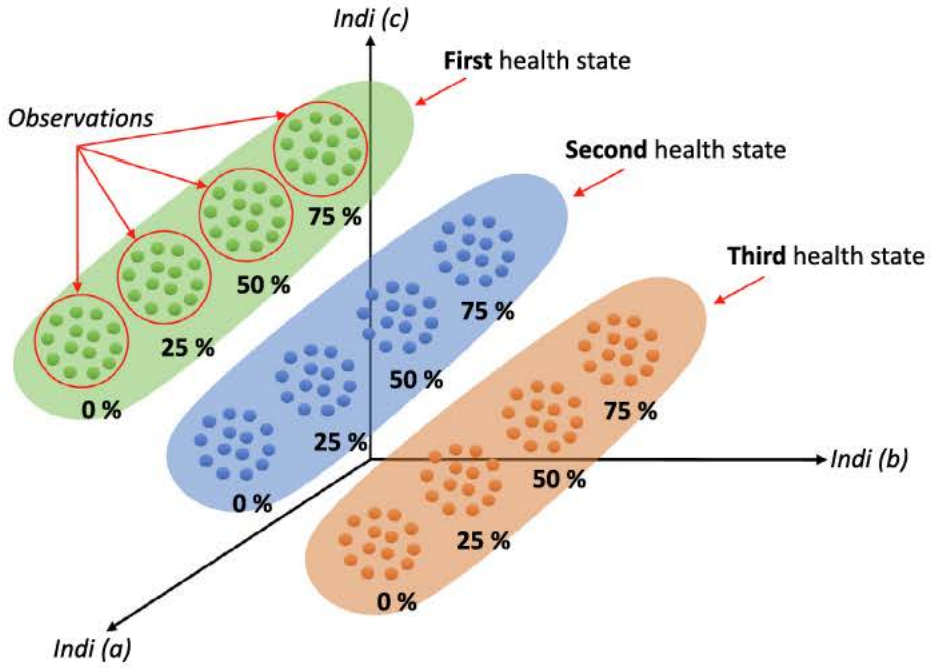


**Fig. 6.** Dispersion of features caused by the variation of load levels.

the training database. In our case, the number of studied classes is equal to 7. Each class is composed of 100 observations. Thus, the number of all observations $N$ is equal to 700. To perform this task, the constructed matrix *indi* is divided into a training database and a test database. The training database is derived from classes named $\Omega_s, 1 \leqslant s \leqslant 7$, where $s$ represents the number of health states of the gearbox components. Each training class is represented by a matrix composed of 50% of observations taken randomly from each class and defined by the vector $(indi_{iah}, indi_{ibh}, indi_{ich})$. The training database corresponds finally to a matrix of $n$ lines ($n$ 350), containing the health indicators observations, and three columns corresponding to the three phase current indicators. This matrix is used to train the classifier model. The test database is also constructed randomly from *indi* and composed of 50% of each class to test the accuracy of the classifier model as illustrated in Fig. 10. The test database corresponds finally to a matrix of $n$ 350 lines.

In the literature, numerous machine learning techniques are used to detect and diagnose bearing and gear defects. Among these techniques, we can cite the most effective methods such as Neural networks (NN) [31,32], K Nearest Neighbors (K NN) [33], Support vector machines (SVM) [31,34,35], Naïve Bayes classifier (NB) [36] and Adaptive Neur Fuzzy Inference System (ANFIS) [37,38,30]. Each of these techniques presents its own advantages and drawbacks. However, as the ANFIS combines both artificial neural networks and fuzzy inference systems, it allows exploiting

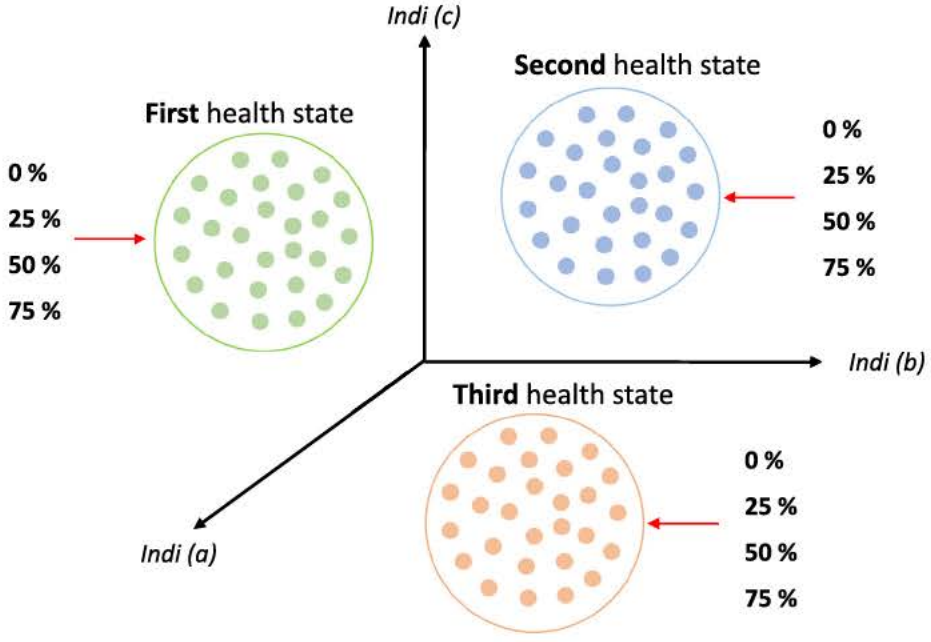


**Fig. 7.** Dispersion limitation thanks to the normalization to the MAX(FFT($y_{jh}$)) value.

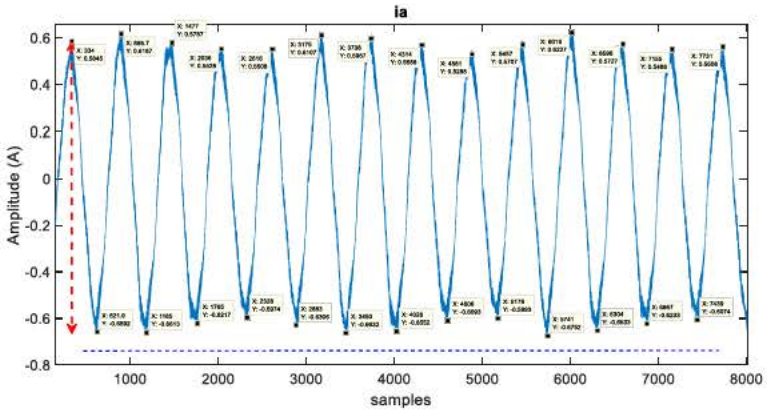


a) Time domain analysis

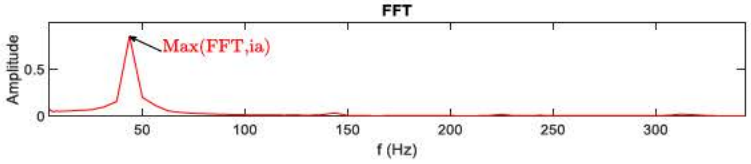


b) Frequency domain analysis

**Fig. 8.** Combination of time and frequency analysis for vectors dispersion limitation.

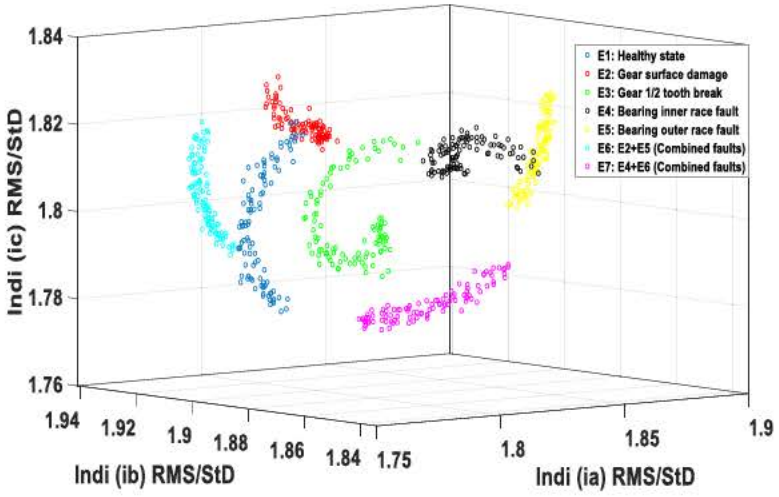


**Fig. 9.** Health indicators construction characterizing different health states.

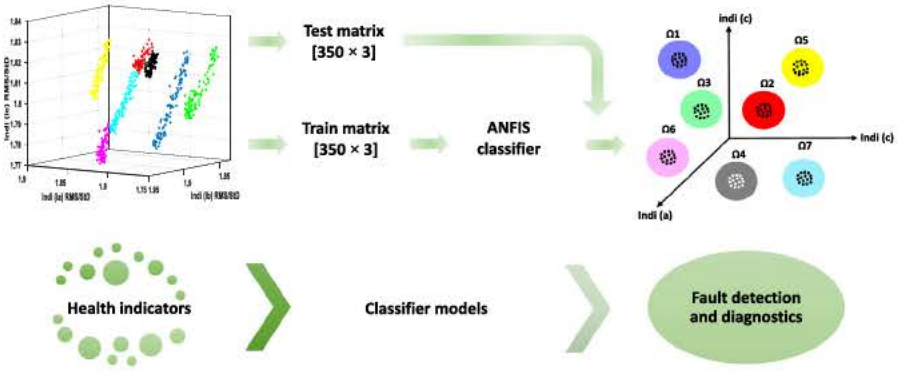


**Fig. 10.** From health indicators to fault detection and diagnostics.

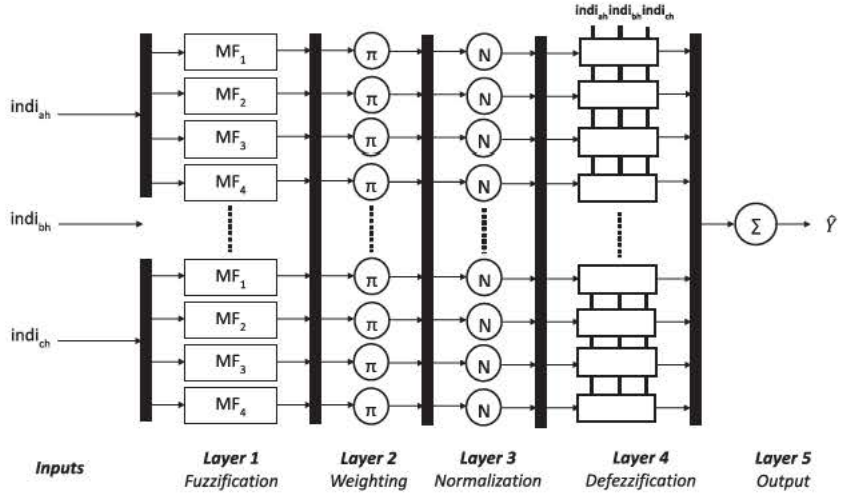


**Fig. 11.** ANFIS structure.

the ability of a neural network to classify and identify patterns with a rule based fuzzy logic model leading to an increase of the learning capacity [39].

The ANFIS was initially developed by [37] in 1993. It is made of five layer neural network, where each layer performs a step of a fuzzy inference system of type Takagi Sugeno, also called (pre neuronal architecture). ANFIS uses the hybrid learning algorithm between the descent gradient method and the least square method to minimize the error between the ANFIS output (prediction val ues) and the target values (true values). The general structure of ANFIS is shown in Fig. 11.

In details, ANFIS has a set of inputs values from the health indi cators observations denoted ($indi_{ah}$, $indi_{bh}$, $indi_{ch}$). These indicators are extracted from the training database that characterizes the dif ferent health states of the gearbox. Each observation of the training matrix is associated to a membership function, which can be trian gular, gaussian, trapezoidal, etc. In our case where four functions are considered, the ANFIS has $j \quad 3^4$ fuzzy rules $\mu$, with 3 is the number of inputs (health indicators = 3), and 4 is the number of membership functions (MF: gauss, gauss2mf ...). These rules can be given as follows:

$$if indi_{ah} \text{ is } \mu_1^j, \quad indi_{bh} \text{ is } \mu_2^j, \text{ and } indi_{ch} \text{ is } \mu_3^j \tag{5}$$

$$\widehat{Y} \quad \sum_{j\ 1}^{3^4} \omega_j f_j(indi_{ah}, indi_{bh}, indi_{ch}) \tag{6}$$

with:

$$f_j(indi_{(a,b,c)h}) \quad \overline{\omega}_j.\left(c_1^j.indi_{ah} + c_2^j.indi_{bh} + c_3^j.indi_{ch} + c_{3+1}^j\right) \tag{7}$$

and where $c$ represents the coefficients of the rule $j$, $\omega$ is the weight of the rule $j$, and $\widehat{Y}$ corresponds to the output of the ANFIS model (the predicted values of the different health states of the motor).

*First layer (Fuzzification)* The first layer contains as many neu rons as possible of the fuzzy subset in the inference system. It per forms the fuzzification of the training input set from ($indi_{ah}$, $indi_{bh}$, $indi_{ch}$), by calculating the membership degree of each input through a membership function.

$$o^1 \quad \mu_{ij}(indi_{(a,b,c)h}) \text{ with } i \quad 1,2 \tag{8}$$

where $\mu_{ij}$ represents the membership functions used for the fuzzi fication. In this paper, the Gaussian function [37] is considered.

*Second layer (Weighting of the fuzzy rules)* The second layer cal culates the activation degree of the premises (output of the first layer), where each neuron in this layer marked $\pi$ corresponds to a fuzzy rule of the type Sugeno. The output of this layer (weights $w_j$) corresponds to the product of the fuzzy inputs. The activation functions used on these neurons depend on the operators AND/ OR cited in Eq. (5).

$$o^2 \quad \omega_j \quad \mu_1^j(indi_{ah}).\mu_2^j(indi_{bh}).\mu_3^j(indi_{ch}) \tag{9}$$

*Third layer (Normalization)* The third layer normalizes the activa tion degree of each rule, i.e. each node in this layer, marked $N$, receives at its input the output of the previous layer of the $i^{th}$ neuron, and then calculates the ratio between the $i^{th}$ rule weight and the sum of all rule weights. The output of this layer is the normalized weights.

$$o^3 \quad \overline{\omega_j} \quad \frac{\omega_j}{\sum_{j\ 1}^{3^4}\omega_j} \tag{10}$$

*Fourth layer (Defuzzification)* The fourth layer ensures the defuzzification of the previous layer to determine the parameters of the activation function $c$, i.e. $c$ is the consequent parameters.

$$o^4 \quad \overline{\omega}_j f_j \quad \overline{\omega}_j.\left(c_1^j.indi_{ah} + c_2^j.indi_{bh} + c_3^j.indi_{ch} + c_{3+1}^j\right) \tag{11}$$

*Fifth layer (Output)* The fifth layer contains a single neuron in a cir cle marked $\sum$. Its role is to calculate the sum of the previous output.

$$o^5 \quad \widehat{Y} \quad \sum_{j\ 1}^{3^4} \overline{\omega}_j.\left(c_1^j.indi_{ah} + c_2^j.indi_{bh} + c_3^j.indi_{ch} + c_{3+1}^j\right) \tag{12}$$

The $\widehat{Y}$ represents the predicted values of the different health states of the motor. These values will be used to evaluate and clas sify the data from the testing set.

## 3. Application and results

This section presents the application used to test and verify the performance and the robustness of the proposed methodology for bearing and gear fault detection and diagnostics. The application consists of a test bench installed at laboratory level (Fig. 12). Three phase current signals are continuously recorded from the output of the pulse generator placed before the motor. These signals are recorded at different operating conditions by varying the speed and the load. They are then processed separately, in frequency and time domains, to show the limits of these traditional approaches and to emphasize the added value of the proposed health indicator. Finally, the obtained health indicators are fed into classifier models to diagnose the motor's bearing and gear health states.

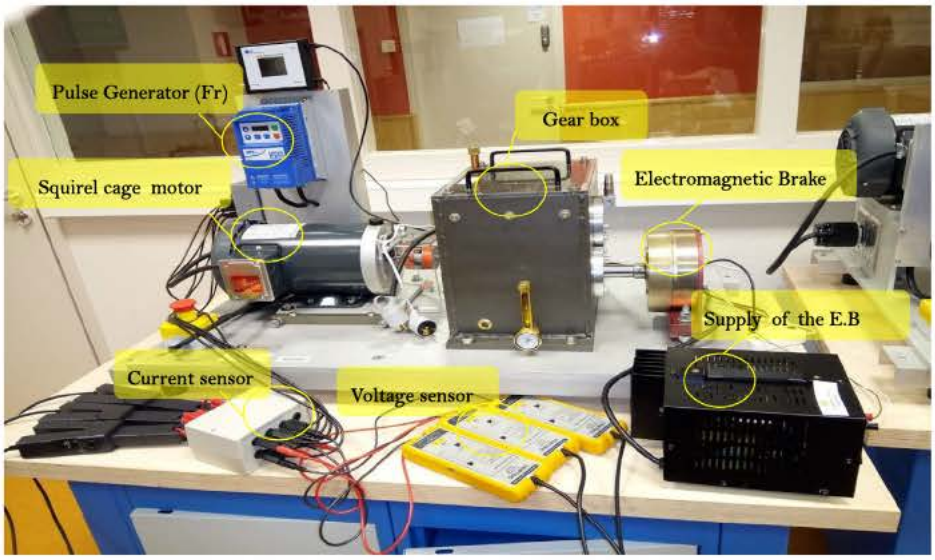


**Fig. 12.** Test bench installed at LASPI laboratory.

### 3.1. Description of the test bench

The Fig. 12 shows the test bench installed at the LASPI laboratory in France. Its overall scheme is presented in Fig. 14. In detail, the asynchronous cage motor drives a three axis gearbox. This latter component is composed of three rotating shafts. The first shaft *AE*, also named as the input shaft, is directly driven by the rotor shaft. At the output shaft, an electromagnetic brake is placed in order to apply a load level to the motor. The second shaft *AI* contains the gear and the bearing components used during the experiments (the green zone in Fig. 14). This shaft is geared by the input shaft. Finally, the third shaft *AS* is named as the output shaft and is geared by the *AI* shaft. The motor is powered by a pulse generator that adjusts its speed by varying the rotating frequencies (25 Hz, 35 Hz and 45 Hz). The achieved experiments correspond to four load levels (0%, 25%, 50% and 75%) at different speeds. Regarding the data acquisition part, the current sensors are installed at the stator level and connected to an acquisition card (reference 9234 from National Instrument) to record the three phase currents. The recorded data are stored in *csv* files by using Matlab software. Each file contains 10 s of the current signal sampled at a frequency equal to 25.6 kHz.

This test bench is dedicated for bearing and gear fault diagnostics. It is equipped with specified components representing different states such as outer and inner race faults in bearings, surface damage and half tooth break faults in gears. The Fig. 15 shows the components used in the experimental tests with different failure types considered in this work.

In this application, seven types of experiments that characterize seven health states of the motor were performed on the test bench. These experiments are summarized in Fig. 13.

Each experiment, from *E*1 to *E*7, required the change of the components mounted between the *AI* and *AS* shafts, as illustrated in Fig. 14. From the Fig. 13, one can see that in the first experiment *E*1, all the components are in a healthy state whereas in the second experiment *E*2 a surface damage is present in the gear at the *AI* shaft.

### 3.2. Investigation on the fault signatures using spectral analysis

This subsection deals with the extraction of the characteristic frequencies corresponding to the component defects. In the case of bearings, the faults can be distributed in different components as shown in Fig. 16.

The vibration caused by these component defects (inner race, outer race, cage and rolling balls) affect the current signals by producing harmonic frequencies due to the radial motion between the motor rotor and the stator. Each defect can be localized through its characteristic frequency by the following equation:

| Gear | | | | | Bearing | | Legend |
|---|---|---|---|---|---|---|---|
| Exp | 29 Teeth | 100 Teeth | 36 Teeth (AI : AS) | 90 Teeth | AI : AS | AI : AE | |
| E1 | Healthy | Healthy | Healthy | Healthy | Healthy | Healthy | Healthy state |
| E2 | Healthy | Healthy | Surface damage | Healthy | Healthy | Healthy | Gear surface damage |
| E3 | Healthy | Healthy | ½ Tooth break | Healthy | Healthy | Healthy | Gear ½ tooth break |
| E4 | Healthy | Healthy | Healthy | Healthy | Inner race | Healthy | Bearing inner race fault |
| E5 | Healthy | Healthy | Healthy | Healthy | Outer race | Healthy | Bearing outer race fault |
| E6 | Healthy | Healthy | Surface damage | Healthy | Inner race | Healthy | Combined fault (E2 + E4) |
| E7 | Healthy | Healthy | ½ Tooth break | Healthy | Outer race | Healthy | Combined fault (E3+ E5) |

**Fig. 13.** List of experiments performed on the test bench.

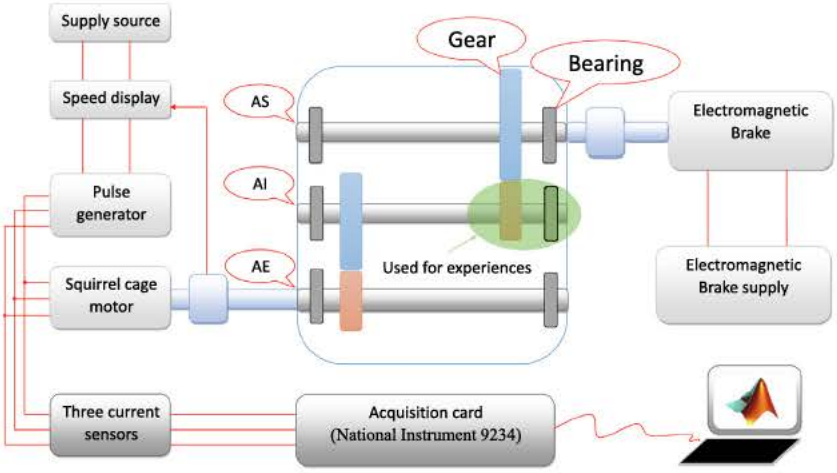


**Fig. 14.** Overall scheme of the test bench.


**Fig. 15.** Illustration of different component experiences.

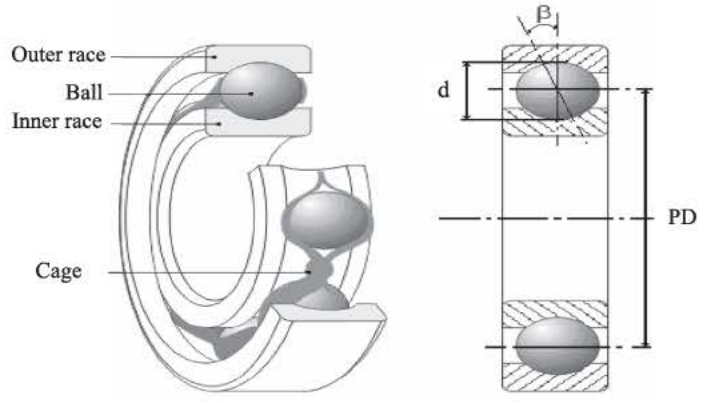


**Fig. 16.** Bearing components.

$$f_{fault} \quad |f_e \pm k f_b| \tag{13}$$

where $f_e$ represents the electrical supply frequency, $k$ $(1, 2, 3 \ldots)$ is the harmonic number generated by the current signals and $f_b$ corresponds to the characteristic frequencies of the bearing elements.

The spectral analysis conducted hereafter aims to show the impossibility of detecting faults by using the characteristic frequencies extracted from the recorded current signals at different operating conditions. However, for illustration and clarity of presentation, only the operating condition corresponding to a

**Table 1**
Characteristic parameters of the bearing used for the experimental tests.

| | |
|---|---|
| Number of rolling elements, *Nr* | 9 |
| Contact angle, $\beta$ (°) | 0 |
| Rotating frequency, $f_r$ (*Hz*) | 43.75 |
| Diameter of the rolling elements, *d* (*inch*) | 0.2762 |
| Pitch diameter, *PD* (*inch*) | 0.7342 |

speed of 45 Hz and a load level of 75% is considered in this application.

The characteristic frequencies of the bearing inner and outer race defects are expressed by Eq. (14) whereas the characteristic parameters of the bearing are given in Table 1.

$$\begin{aligned} &\texttt{Inner race} \quad f_{ir} \quad \frac{Nr}{2}\left[1 \quad \frac{d.\cos(\beta)}{PD}\right].f_r \\ &\texttt{Outer race} \quad f_{or} \quad \frac{Nr}{2}\left[1+\frac{d.\cos(\beta)}{PD}\right].f_r \end{aligned} \tag{14}$$

where *Nr* is the number of rolling elements, *d* represents the rolling elements diameter, *PD* is the pitch diameter, $\beta$ represents the contact angle.

The above fault characteristic frequencies (inner race and outer race defects) are calculated by the information presented in the Table 1. Therefore, the inner race frequency is $f_{ir}$ 276.319 Hz, and the outer race frequency is $f_{or}$ 125.231 Hz.

The Fig. 17 shows the spectrum of the current signal in the cases of a healthy and a faulty bearing. From these figures, one can notice that the magnitude at the harmonic frequencies of the defect bearing is different when compared with the ones calculated above. Therefore, one can conclude that the defects cannot be detected by using this technique. To remedy to this situation, the proposed health indicator is applied in the following subsection.

### 3.3. Health indicators construction

In this application, seven experimental tests (see Fig. 13) were performed for different operating conditions to acquire the three phase current signals and extract health indicators. These indicators are then used to evaluate the performance and the robustness of the methodology proposed in Section 2.

First, the performance of the proposed health indicator RMS/StD is highlighted against the health indicators using only root mean square (RMS), variance (VAR) and kurtosis (KUR) values, which are the most employed features in the literature. Thus, seven classes corresponding to the motor's bearing and gear health states (char

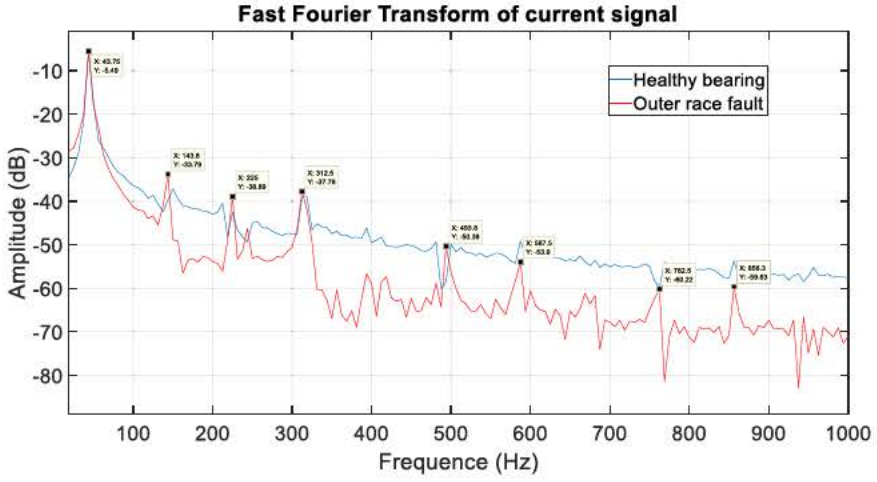


a) Outer race defect

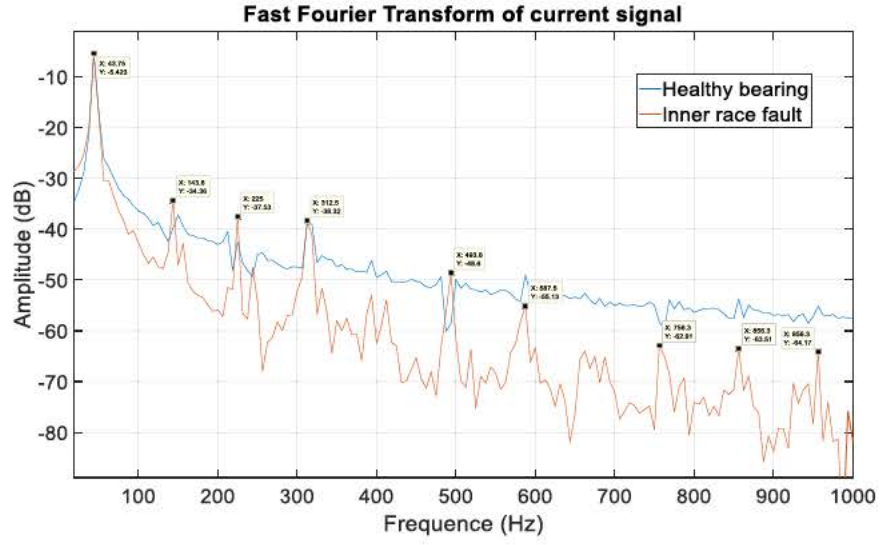


b) Inner race defect

**Fig. 17.** Comparison of the spectrum between healthy case and faulty case.

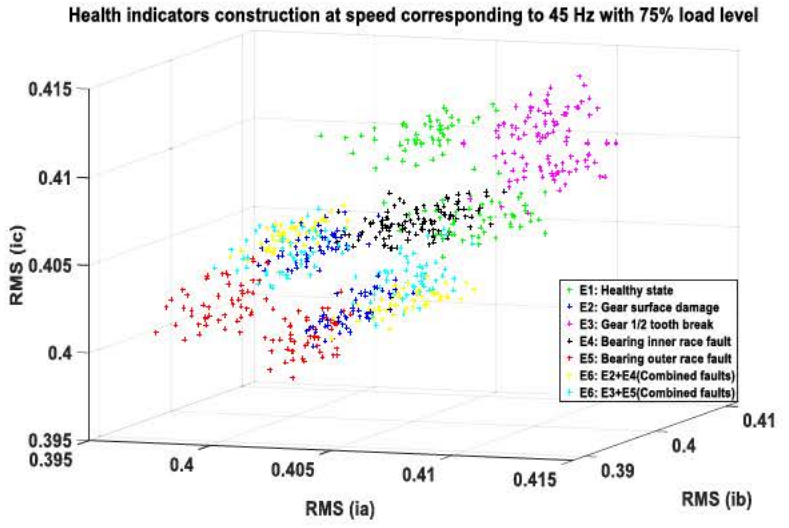


Fig. 18. Health indicators construction using RMS values.

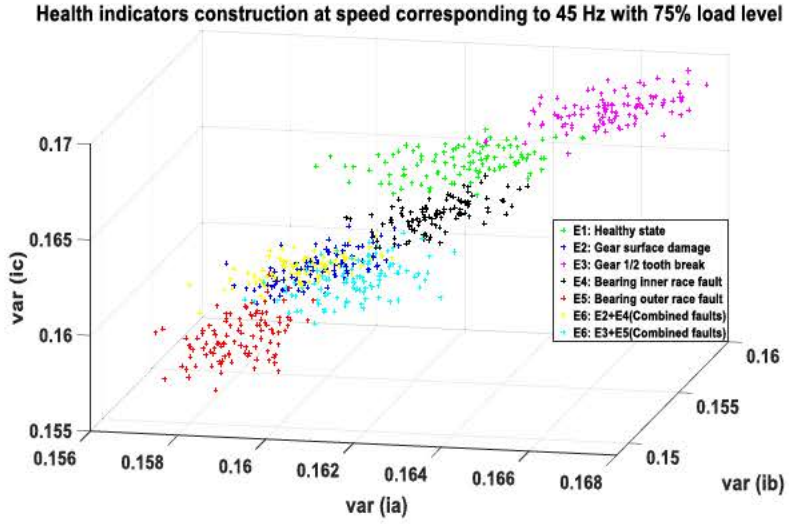


Fig. 19. Health indicators construction using VAR values.

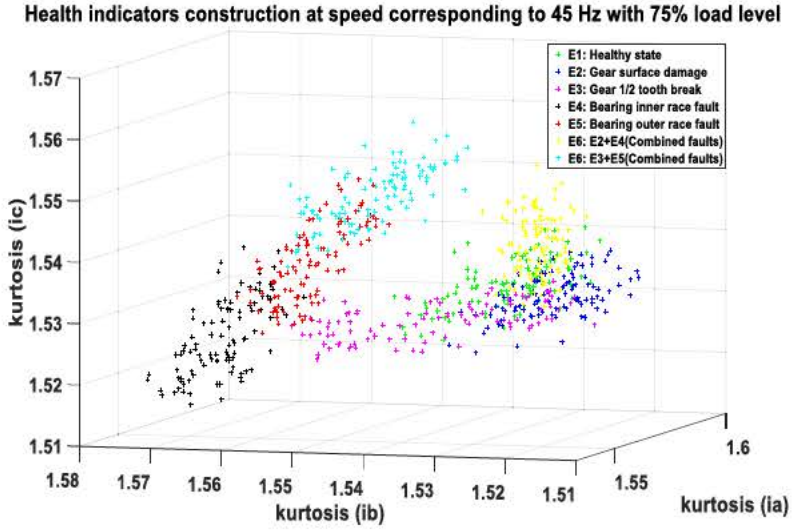


Fig. 20. Health indicators construction using KUR values.

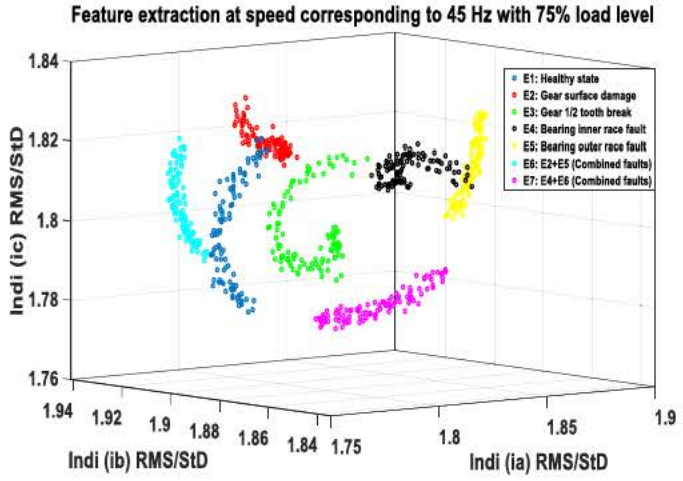


a) Speed corresponding to 45 Hz

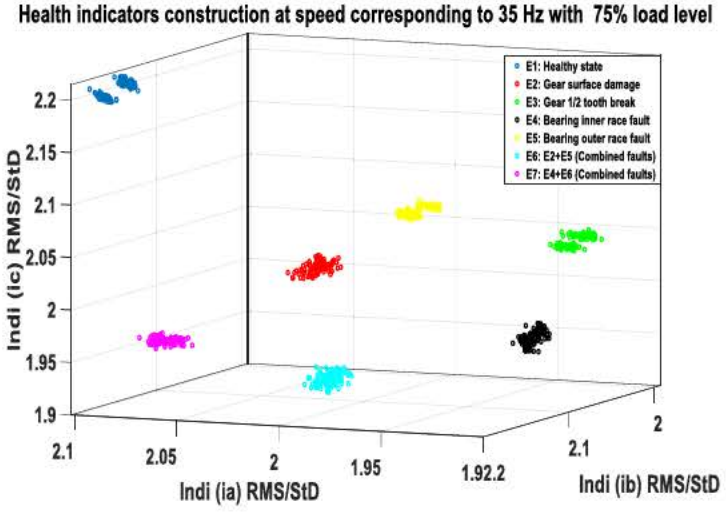


b) Speed corresponding to 35 Hz

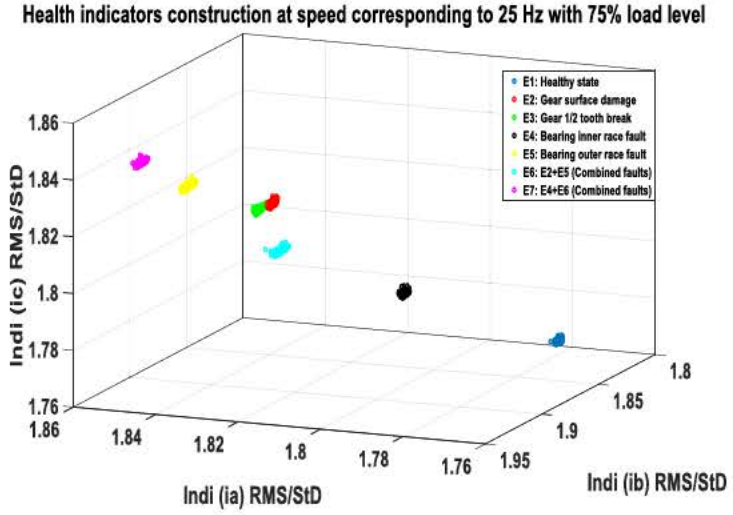


c) Speed corresponding to 25 Hz

**Fig. 21.** Distribution of the health indicators at 75% of load.

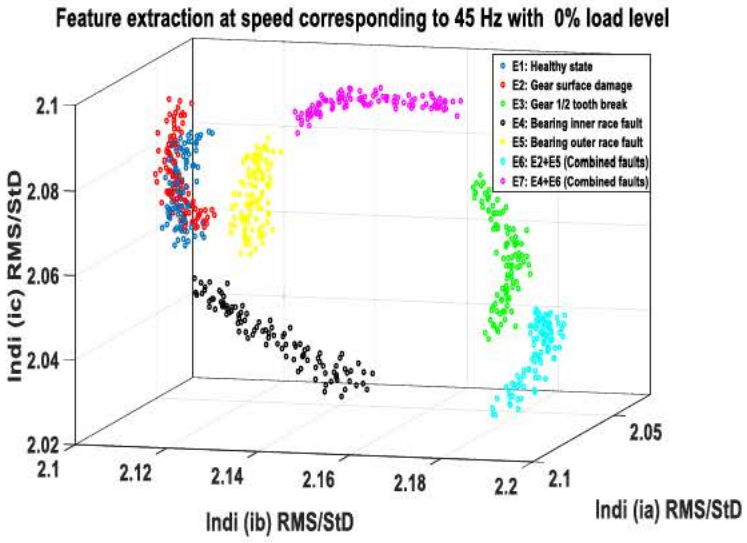


Speed corresponding to 45 Hz

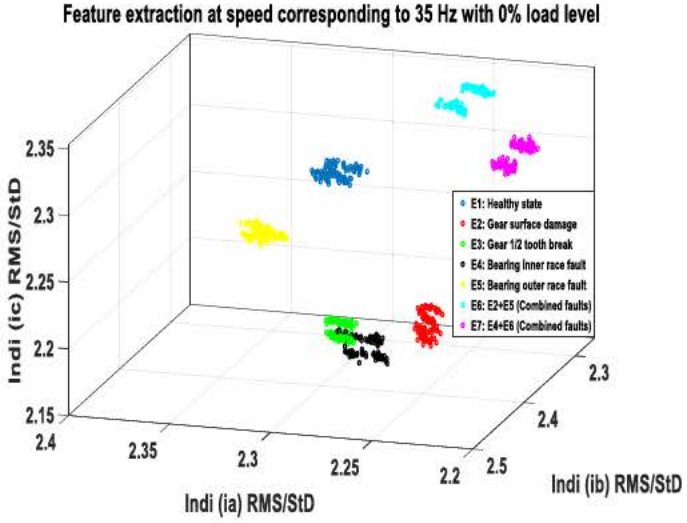


Speed corresponding to 35 Hz

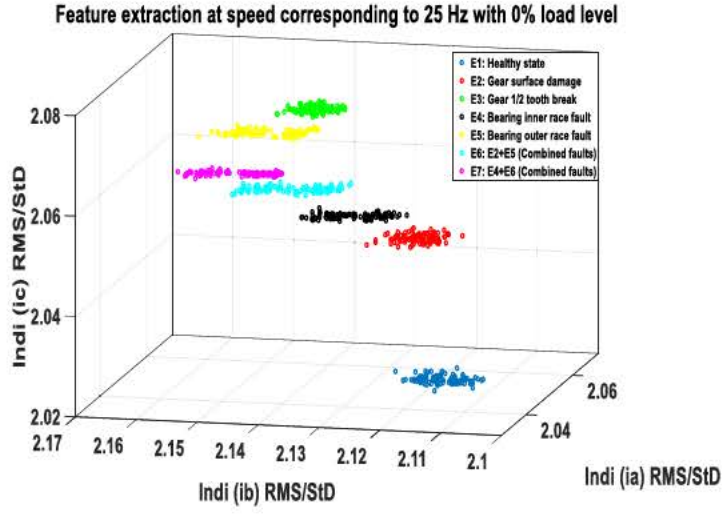


Rotating frequency = 25 Hz

**Fig. 22.** Distribution of the health indicators at no load level test (0%).

**Table 2**
Accuracy score (%) comparison between the classifiers at different operating conditions of the motor. 9 operating conditions: C1 (45 Hz, 75% load), C2 (45 Hz, 50% load, C3 (45 Hz, 25% load), C4 (35 Hz, 75%load), C5 (35 Hz, 50%load), C6 (35 Hz, 25% load), C7 (25 Hz, 75% load, C8 (25 Hz, 50% load), and C9 (25 Hz, 25% load) represent the 9 operating conditions of the motor. 7 classifiers: RF (Random Forest), SVM (Support Vector Machine), LR (Logistic Regression), NB (Naïve Bayes), DT (Decision Tree), KNN (K-Nearest Neighbors), LDA (Linear Discriminant Analysis), and ANFIS (Adaptive Neuro-Fuzzy Inference System).

| Case | C1 | C2 | C3 | C4 | C5 | C6 | C7 | C8 | C9 |
|---|---|---|---|---|---|---|---|---|---|
| RF | 99.42 | 99.14 | 93.42 | **100** | 99.42 | 99.71 | **100** | 99.72 | 99.71 |
| SVM | **100** | 92.28 | 80.57 | **100** | **100** | **100** | 82.28 | 66.57 | **100** |
| LR | 98.28 | 87.42 | 72.28 | **100** | **100** | 90.28 | 70 | 63.42 | **100** |
| NB | 99.71 | 95.42 | 85.14 | **100** | **100** | **100** | **100** | 99.71 | **100** |
| DT | 99.71 | 98.57 | 88.28 | **100** | 99.71 | 97.42 | **100** | 99.14 | **100** |
| KNN | **100** | **100** | 94.58 | **100** | **100** | **100** | **100** | 99.71 | **100** |
| LDA | **100** | **100** | 90 | **100** | **100** | 99.42 | **100** | 99.71 | **100** |
| ANFIS | **100** | **100** | **95** | **100** | **100** | **100** | **100** | **100** | **100** |

acterized by seven colors shown in Fig. 13) and using only RMS, VAR and KUR values are shown in Figs. 18 20 respectively.

These figures show a wide dispersion of the health indicators using only RMS, VAR and KUR. Thus, one can conclude that their utilization is not sufficient to detect different health states of the gearbox. On the other side, the performance of our proposed health indicator when considering 25 Hz, 35 Hz, 45 Hz and 75% of load level is shown in Fig. 21.

From Fig. 21, it can be seen that the proposed health indicator allows clearly separating seven classes corresponding to the gear box health states in different operating conditions, 45 Hz, 35 Hz and 25 Hz with 75% load level. The class separability for the speeds corresponding to 25 Hz and 35 Hz of the pulse generator is higher than the one of the speed corresponding to 45 Hz. In addition, the robustness of the proposed health indicator is highlighted in the cases of 25 Hz, 35 Hz and 45 Hz with 0% load level.

The Fig. 22 shows a negligible dispersion of the extracted health indicators and a clear separability between the classes with numerous operating conditions of the motor (different load and speed levels). These results highlight the efficiency of the proposed health indicator to characterize the different health states of the gearbox by using the current signals, even in the cases of low load levels.

### 3.4. Fault classification

The health indicators extracted previously are used in this sub section to diagnose the bearing and the gear faults at different operating conditions of the motor by varying the load and the speed levels. For this purpose, the health indicator vectors obtained in subSection 2.2 are fed into the input of the ANFIS classifier. The structure of these vectors is shown hereafter.

$$indi = \begin{bmatrix} N & indi_{ia} & indi_{ib} & indi_{ic} & \Omega_s \\ 1 & 1.7849 & 1.8992 & 1.7789 & 1 \\ 2 & 1.7871 & 1.8989 & 1.7817 & 1 \\ \dots & \dots & \dots & \dots & \dots \\ 298 & 1.7628 & 1.8372 & 1.8201 & 3 \\ 299 & 1.7653 & 1.8416 & 1.8233 & 3 \\ \dots & \dots & \dots & \dots & \dots \\ 699 & 1.8387 & 1.9171 & 1.7709 & 7 \\ 700 & 1.8399 & 1.9201 & 1.7727 & 7 \end{bmatrix}$$

where N is the number of training and test observations, $\Omega_s$ is the membership class and $1 \leqslant s \leqslant 7$ (the seven health states of the motor's bearing and gear).

These vectors are then divided into a training set and a test set, both are chosen randomly from the total observations of the con structed matrix *indi*. Note that each health indicator contains three values corresponding to the three phase currents.

In order to prove the efficiency of the ANFIS classifier model, its classification results are compared to those obtained by other clas sifiers (RF, SVM, LR, NB, DT, KNN and LDA) with the obtained matrix *indi*. In addition, the robustness of the ANFIS based classifi cation is verified by considering nine operating conditions (C1...C9), which correspond to different load and speed levels. These condition variations impact the health indicator results by reducing the separability between the classes. Therefore, it is nec essary to train a classifier to better diagnose the bearing and gear faults, independently to the operating conditions. The Table 2 sum marizes the performance comparison between the ANFIS and some of the classifiers proposed in the literature. This comparison is based on the health indicator extracted from the current signals. As a reminder, the training and the test data sets are taken ran domly (50% 50%) from the observations of the matrix *indi*, as explained in subSection 2.3.

Based on the Table 2, one can notice that the best classification results are marked in bold. In addition, in all the cases, the accuracy score given by the ANFIS classifier is higher than that one given by the other classifiers. We can also see that the accuracy score of the ANFIS classifier is high and equals to 95% even in the worst case when the motor runs at a high speed with a low load level (C3). For all remaining cases, the accuracy score of ANFIS is equal to 100%. These results highlight the robustness of the proposed diag nostic method under different operating conditions. Indeed, when the motor runs at a high speed (35 Hz or 45 Hz), the accuracy of the other classifier models decreases with the diminution of the load level. For example, at the speed corresponding to 45 Hz, the accu racy score of the LR classifier decreases from 98.28% to 72.28% when the load level reduces from 75% to 25%. These results can be explained by the diminution of the vibration sensitivity, which causes an imbalance of the current signals in the case of defects at high speed and low load condition.

## 4. Conclusion

A methodology based on the three phase current signals has been presented in this paper for fault detection and diagnostics of bearing and gear components. First, a set of relevant features was extracted from the three phase current signals of an asyn chronous motor. These features are then used to build health indi cators that allow separating the different states of the bearing and gear components, taking into account the impact of the operating conditions of the asynchronous motor. Finally, the constructed health indicators were fed into an ANFIS model to classify the dif ferent health states of the bearing and the gear. The proposed methodology was applied on real data taken from an experimental test bench realized at the laboratory level. The obtained results highlighted the performance of the proposed health indicator to detect and diagnose different faults of the bearing and gear. Fur thermore, the robustness of the proposed methodology was veri

fied through the detection of simultaneous faults of the bearing and the gear under different motor speed and load levels. The accu racy of the ANFIS model was also compared to that of numerous classifiers proposed in the literature. This comparison clearly showed the superiority of the ANFIS model.

As a limit of the proposed diagnostic methodology, one can mention the fact that it is a supervised one. Therefore, it requires historical data to learn the fault patterns before diagnosing them, which may be difficult to obtain in some industrial cases.

As future work, more fault types, such as the combination between bearing and gear faults and also the combination between mechanical and electrical defects, will be investigated. The applica tion of the proposed methodology on other types of motors could be also a good perspective to show its effectiveness.

## References


[1] R. Gouriveau, K. Medjaher, N. Zerhouni, From Prognostics and Health Systems Management to Predictive Maintenance 1: Monitoring and Prognostics, John Wiley & Sons, 2016.

[2] V. Atamuradov, K. Medjaher, P. Dersin, B. Lamoureux, N. Zerhouni, Prognostics and health management for maintenance practitioners-review, implementation and tools evaluation, Int. J. Progn. Health Manage. 8 (060) (2017) 1–31.

[3] A. Soualhi, K. Medjaher, N. Zerhouni, H. Razik, Early detection of bearing faults by the hilbert-huang transform, in: Control Engineering & Information Technology (CEIT), 2016 4th International Conference on, IEEE, 2016, pp. 1–6.

[4] R. Shao, W. Hu, Y. Wang, X. Qi, The fault feature extraction and classification of gear using principal component analysis and kernel principal component analysis based on the wavelet packet transform, Measurement 54 (2014) 118–132, https://doi.org/10.1016/j.measurement.2014.04.016.

[5] D. Lu, W. Qiao, X. Gong, Current-based gear fault detection for wind turbine gearboxes, IEEE Trans. Sustainable Energy 8 (4) (2017) 1453–1462.

[6] Y. Zhang, C. Zhang, J. Sun, J. Guo, Improved wind speed prediction using empirical mode decomposition, Adv. Electr. Comput. Eng. 18 (2) (2018) 3–11.

[7] Y. Zhang, B. Chen, Y. Zhao, G. Pan, Wind speed prediction of ipso-bp neural network based on lorenz disturbance, IEEE Access 6 (2018) 53168–53179.

[8] M.D. Prieto, G. Cirrincione, A.G. Espinosa, J.A. Ortega, H. Henao, Bearing fault detection by a novel condition-monitoring scheme based on statistical-time features and neural networks, IEEE Trans. Ind. Electron. 60 (8) (2013) 3398–3407, https://doi.org/10.1109/TIE.2012.2219838.

[9] S. Shukla, R. Yadav, J. Sharma, S. Khare, Analysis of statistical features for fault detection in ball bearing, in: Computational Intelligence and Computing Research (ICCIC), 2015 IEEE International Conference on, IEEE, 2015, pp. 1–7.

[10] S. Liu, S. Hou, K. He, W. Yang, L-kurtosis and its application for fault detection of rolling element bearings, Measurement 116 (2018) 523–532.

[11] R.R. Schoen, T.G. Habetler, F. Kamran, R.G. Bartfield, Motor bearing damage detection using stator current monitoring, IEEE Trans. Ind. Appl. 31 (6) (1995) 1274–1279, https://doi.org/10.1109/28.475697.

[12] J.R. Stack, T.G. Habetler, R.G. Harley, Bearing fault detection via autoregressive stator current modeling, IEEE Trans. Ind. Appl. 40 (3) (2004) 740–747, https://doi.org/10.1109/TIA.2004.827797.

[13] J. Zhang, J.S. Dhupia, C.J. Gajanayake, Stator current analysis from electrical machines using resonance residual technique to detect faults in planetary gearboxes, IEEE Trans. Industr. Electron. 62 (9) (2015) 5709–5721, https://doi.org/10.1109/TIE.2015.2410254.

[14] S.H. Kia, H. Henao, G.A. Capolino, Fault index statistical study for gear fault detection using stator current space vector analysis, IEEE Trans. Ind. Appl. 52 (6) (2016) 4781–4788, https://doi.org/10.1109/TIA.2016.2600596.

[15] A. Glowacz, W. Glowacz, Vibration-based fault diagnosis of commutator motor, Shock Vibr. 2018 (2018) 1–10.

[16] L.S. Dhamande, M.B. Chaudhari, Compound gear-bearing fault feature extraction using statistical features based on time-frequency method, Measurement 125 (2018) 63–77.

[17] C. Wang, M. Gan, C. Zhu, A supervised sparsity-based wavelet feature for bearing fault diagnosis, J. Intell. Manuf. (2016) 1–11.

[18] C. Wang, M. Gan, C. Zhu, Fault feature extraction of rolling element bearings based on wavelet packet transform and sparse representation theory, J. Intell. Manuf. 29 (4) (2018) 937–951.

[19] C. Wu, T. Chen, R. Jiang, L. Ning, Z. Jiang, A novel approach to wavelet selection and tree kernel construction for diagnosis of rolling element bearing fault, J. Intell. Manuf. 28 (8) (2017) 1847–1858.

[20] V.C.M.N. Leite, J.G.B.d. Silva, G.F.C. Veloso, L.E.B.d. Silva, G. Lambert-Torres, E.L. Bonaldi, L.E.d.L.d. Oliveira, Detection of localized bearing faults in induction machines by spectral kurtosis and envelope analysis of stator current, IEEE Trans. Ind. Electron. 62 (3) (2015) 1855–1865, https://doi.org/10.1109/TIE.2014.2345330.

[21] S. Singh, N. Kumar, Detection of bearing faults in mechanical systems using stator current monitoring, IEEE Trans. Ind. Inf. 13 (3) (2017) 1341–1349, https://doi.org/10.1109/TII.2016.2641470.

[22] L. Hong, J.S. Dhupia, A time domain approach to diagnose gearbox fault based on measured vibration signals, J. Sound Vib. 333 (7) (2014) 2164–2180, https://doi.org/10.1016/j.jsv.2013.11.033.

[23] S. Fedala, D. Rémond, R. Zegadi, A. Felkaoui, Contribution of angular measurements to intelligent gear faults diagnosis, J. Intell. Manuf. 29 (5) (2018) 1115–1131.

[24] A. Glowacz, Acoustic-based fault diagnosis of commutator motor, Electronics 7 (11) (2018) 299.

[25] A. Glowacz, Recognition of acoustic signals of commutator motors, Appl. Sci. 8 (12) (2018) 2630.

[26] A. Glowacz, Fault diagnosis of single-phase induction motor based on acoustic signals, Mech. Syst. Signal Process. 117 (2019) 65–80.

[27] O.V. Thorsen, M. Dalva, A survey of faults on induction motors in offshore oil industry, petrochemical industry, gas terminals, and oil refineries, IEEE Trans. Ind. Appl. 31 (5) (1995) 1186–1196.

[28] W.T. Thomson, M. Fenger, Current signature analysis to detect induction motor faults, IEEE Ind. Appl. Mag. 7 (4) (2001) 26–34.

[29] O. Ondel, G. Clerc, E. Boutleux, E. Blanco, Fault detection and diagnosis in a set 'inverter–induction machine' through multidimensional membership function and pattern recognition, IEEE Trans. Energy Convers. 24 (2) (2009) 431–441.

[30] A. Soualhi, S. Taleb, Data fusion for fault severity estimation of ball bearings, IEEE International Conference on Industrial Technology (ICIT) 2018 (2018) 2105–2110, https://doi.org/10.1109/ICIT.2018.8352514.

[31] P. Konar, P. Chattopadhyay, Bearing fault detection of induction motor using wavelet and Support Vector Machines (SVMs), Appl. Soft Comput. 11 (6) (2011) 4203–4211, https://doi.org/10.1016/j.asoc.2011.03.014.

[32] T. Dalstein, B. Kulicke, Neural network approach to fault classification for high speed protective relaying, IEEE Trans. Power Delivery 10 (2) (1995) 1002–1011.

[33] T. Cover, P. Hart, Nearest neighbor pattern classification, IEEE Trans. Inf. Theory 13 (1) (1967) 21–27.

[34] S. Abbasion, A. Rafsanjani, A. Farshidianfar, N. Irani, Rolling element bearings multi-fault classification based on the wavelet denoising and support vector machine, Mech. Syst. Signal Process. 21 (7) (2007) 2933–2945.

[35] K. Salahshoor, M. Kordestani, M.S. Khoshro, Fault detection and diagnosis of an industrial steam turbine using fusion of SVM (support vector machine) and ANFIS (adaptive neuro-fuzzy inference system) classifiers, Energy 35 (12) (2010) 5472–5482.

[36] S. Xu, Bayesian naïve bayes classifiers to text classification, J. Inf. Sci. 44 (1) (2018) 48–59.

[37] J.S.R. Jang, ANFIS: adaptive-network-based fuzzy inference system, IEEE Trans. Syst. Man Cybern. 23 (3) (1993) 665–685, https://doi.org/10.1109/21.256541.

[38] Y. Lei, Z. He, Y. Zi, Q. Hu, Fault diagnosis of rotating machinery based on multiple ANFIS combination with GAs, Mech. Syst. Signal Process. 21 (5) (2007) 2280–2294, https://doi.org/10.1016/j.ymssp.2006.11.003.

[39] M. Şahin, R. Erol, A comparative study of neural networks and anfis for forecasting attendance rate of soccer games, Math. Comput. Appl. 22 (4) (2017) 43.